Isoscalar response of ^{68}Ni to α-particle and deuteron probes

M. Vandebrouck, J. Gibelin, E. Khan, N.L. Achouri, H. Baba, D. Beaumel, Y. Blumenfeld, M. Caamano, L. Caceres, G. Colo, et al.

Isoscalar response of ^{68}Ni to alpha-particle and deuteron probes

M. Vandebrouck,[1,2,3] J. Gibelin,[2] E. Khan,[1] N. L. Achouri,[2] H. Baba,[4] D. Beaumel,[1] Y. Blumenfeld,[1] M. Caamaño,[5] L. Càceres,[3] G. Colò,[6] F. Delaunay,[2] B. Fernandez-Dominguez,[5] U. Garg,[7] G. F. Grinyer,[3] M. N. Harakeh,[8,3] N. Kalantar-Nayestanaki,[8] N. Keeley,[9] W. Mittig,[10] J. Pancin,[3] R. Raabe,[11] T. Roger,[11,3] P. Roussel-Chomaz,[12] H. Savajols,[3] O. Sorlin,[3] C. Stodel,[3] D. Suzuki,[10,1] and J. C. Thomas[3]

[1] *IPN Orsay, Université Paris Sud, IN2P3-CNRS, F-91406 Orsay Cedex, France*
[2] *LPC Caen, ENSICAEN, Université de Caen, CNRS/IN2P3, CAEN, France*
[3] *Grand Accélérateur National d'Ions Lourds (GANIL), CEA/DSM-CNRS/IN2P3, Bvd Henri Becquerel, 14076 Caen, France*
[4] *RIKEN Nishina Center, 2-1 Hirosawa, Wako, Saitama 351-0198, Japan*
[5] *Universidade de Santiago de Compostela, E-15706 Santiago de Compostela, Spain*
[6] *Dipartimento de Fisica, Università degli Studi di Milano and INFN, Sezione di Milano, 20133 Milano, Italy*
[7] *Physics Department, University of Notre Dame, Notre Dame, Indiana 46556, USA*
[8] *KVI-CART, University of Groningen, NL-9747 AA Groningen, The Netherlands*
[9] *National Centre for Nuclear Research, ul. Andrzeja Sołtana 7, 05-400 Otwock, Poland*
[10] *NSCL, Michigan State University, East Lansing, Michigan 48824-1321, USA*
[11] *Instituut voor Kern- en Stralingsfysica, KU Leuven, B-3001 Leuven, Belgium*
[12] *CEA-Saclay DSM, F-91191 Gif sur Yvette Cedex, France*

Isoscalar giant resonances have been measured in the unstable ^{68}Ni nucleus using inelastic alpha and deuteron scattering at 50A MeV in inverse kinematics with the active target MAYA at GANIL. Using alpha scattering, the extracted isoscalar giant monopole resonance (ISGMR) centroid was determined to be 21.1 ± 1.9 MeV and the isoscalar giant quadrupole resonance (ISGQR) to be 15.9 ± 1.3 MeV. Indications for soft isoscalar monopole and dipole modes are provided. Results obtained with both (α,α') and (d,d') probes are compatible. The evolution of isoscalar giant resonances along the Ni isotopic chain from ^{56}Ni to ^{68}Ni is discussed.

PACS numbers: 21.10.Re,24.30.Cz,21.60.Jz,24.50.+g,21.60.Ev

I. INTRODUCTION

Measurement of the isoscalar giant resonances (ISGR), and in particular the isoscalar giant monopole resonance (ISGMR) plays an important role in constraining the nuclear equation of state [1]. More precisely, the energy of the ISGMR, that corresponds to a succession of compression/expansion phases of the atomic nucleus, also called the breathing mode, where all the protons and neutrons oscillate in phase, can be linked to the nuclear-matter incompressibility. The nuclear-matter incompressibility has been constrained in the last decades using measurements in stable nuclei that are made up only with symmetric matter or slightly asymmetric matter (in a local density approximation picture). However, measurements in unstable nuclei are lacking in order to study the evolution of the nuclear-matter incompressibility as a function of the neutron-proton asymmetry. Recently, it has been shown that measuring the energy of the ISGMR provides information on the ability to compress the matter around the average density of nuclei, which is typically 70% of the saturation density [2, 3]. The present work emphasizes the importance of measuring the ISGMR in different nuclei at several neutron-proton asymmetries and several densities.

Moreover, an isoscalar monopole mode at lower energy, called soft monopole mode, has been predicted in neutron-rich nuclei by several relativistic and non-relativistic models [4–6]. Recently calculations with an exact treatment of the continuum [7] have also predicted monopole strength in the same energy region. However, this mode is found to be characterized with a larger width and turns out to originate mainly from the continuum background. Such a soft monopole mode has not yet been observed.

Experimentally, the measurement of giant resonances in unstable nuclei is a challenging task which has until now been mainly dedicated to the study of the isovector giant dipole resonance (IVGDR) and the isovector pygmy dipole resonance (IVPDR). Photons being a relevant probe to excite the IVGDR and the IVPDR, Coulomb excitation with absorption of a virtual photon has been used, for example, to study the IVGDR and IVPDR in neutron-rich O, Ne, Sn isotopes and in ^{68}Ni [11]. In these studies, the invariant-mass method was used, requiring the detection of all the decay products. These experiments yielded evidence for the appearance of a low-energy dipole mode the nature of which is still under discussion; it may correspond to an oscillation of a neutron skin against a nucleus core and possibly mixed with isoscalar dipole strength [12, 13].

In the case of the isoscalar response, the first measurement was performed on the $N = Z$ unstable ^{56}Ni nucleus and deuteron as probe. The ISGMR has been measured at 19.3 ± 0.5 MeV and the isoscalar giant quadrupole resonance (ISGQR) at 16.2 ± 0.5 MeV [14]. The isoscalar giant dipole resonance (ISGDR), a second-order mode corresponding to the so-called squeezing mode [8, 9], has

never been measured in an unstable nucleus. It should be noted that in Ref. [10], relativistic random-phase approximation (RRPA) calculations indicate some substantial isoscalar dipole strength in ^{68}Ni.

Measuring the scattering of radioactive nuclei from light probes requires the use of inverse kinematics and the detection of very low-energy light charged particles. Therefore, a pioneering technique, using an active target as a detector and the missing-mass method, has been developed for measuring the ISGR with a deuteron probe [14]. This innovative technique has been used again for the present experiment and will be described below.

In addition to the challenge of measuring for the first time the ISGR in a neutron-rich nucleus, there are other goals for this study. These are *i*) to understand the evolution of the nuclear-matter incompressibility along an isotopic chain, and *ii*) to check for the prediction of a soft monopole mode as well as the prediction of a soft isoscalar dipole mode in neutron-rich nuclei. As a soft monopole mode is predicted in ^{68}Ni [4, 5, 7] and as the only measurement of ISGR in an unstable nucleus has been done in ^{56}Ni [14], ^{68}Ni is a nucleus of choice in order to address these questions. Therefore, we present here the first measurement of the isoscalar giant resonances in a neutron-rich unstable nucleus, ^{68}Ni.

The experiment was performed at Grand Accelérateur National d'Ions Lourds (GANIL), Caen, France. During a first part, the active target with filled with He gas to study the inelastic scattering of ^{68}Ni on alpha particles, and during a second part, the active target was filled with D_2 gas to study inelastic scattering on deuteron. Both measurements were performed with a ^{68}Ni beam at an energy of 50A MeV. In the present work, the analysis of the ISGR using both the alpha and the deuteron inelastic scattering will be reported. Some of the results on the isoscalar monopole response with the alpha-particle probe presented here have previously been published [15].

Section II introduces the experimental setup and the techniques used to study giant resonances using an active target. In section III and IV, the results for the ^{68}Ni(α,α')^{68}Ni* and ^{68}Ni(d,d')^{68}Ni* experiments are presented and, finally discussed in section V.

II. EXPERIMENTAL SETUP AND ANALYSIS

A. Experimental setup

The ^{68}Ni beam at 50A MeV was obtained by fragmentation of ^{70}Zn at GANIL. The beam, with an energy of 62.3A MeV, impinged on a ^{9}Be fragmentation target of 29 mg/cm^2 thickness and the ^{68}Ni was selected using the Ligne d'Ions Super Epluchés (LISE) spectrometer [16]. A 560 μm thick achromatic degrader of ^{9}Be was placed between the two LISE dipoles. The average beam intensity of ^{68}Ni was 4×10^4 pps with a purity of $75\% \pm 6\%$.

Isoscalar giant resonances are best studied using inelastic scattering of isoscalar particles around 50A MeV [1] with, for example, alpha or deuteron probes. The use of the (α,α') reaction to study isoscalar giant resonances provided useful results in stable nuclei like in the Sn isotopic chain, for example [17]. When studying unstable nuclei, inverse kinematics must be used with the unstable beam impinging on a He or D target which entails additional technical difficulties.

Figure 1 displays the inelastic scattering angular distributions calculated within the distorted-wave-Born approximation (DWBA). Transition densities for ^{68}Ni were calculated within the microscopic random-phase approximation (RPA) [18] using the Skyrme SkI2 interaction [19] with a nuclear-matter incompressibility $K_\infty = 241$ MeV. The code Fresco [20] was used to calculate the angular distributions with diagonal and transition potentials calculated using the code Dfpot [21]. For the ^{68}Ni(α,α')^{68}Ni* reaction the potentials were generated using the single-folding model and a Gaussian nucleon-alpha interaction with parameters determined from fitting the ^{64}Ni(α,α) elastic scattering data at 43A MeV [22] with a similar procedure. For the ^{68}Ni(d,d')^{68}Ni* reaction the potentials were determined microscopically within the double-folding model using the M3Y effective nucleon-nucleon interaction and a deuteron density calculated with the Hulthén wave function [23].

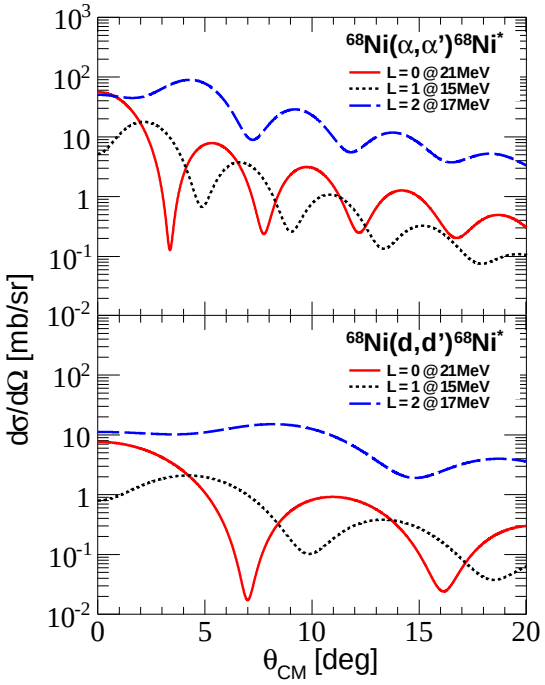

FIG. 1. (Color online) Angular distribution predictions calculated in the DWBA approximation for the monopole excitation at 21 MeV, the dipole at 15 MeV and the quadrupole at 17 MeV. Top: For the ^{68}Ni(α,α')^{68}Ni* reaction. Bottom: For the ^{68}Ni(d,d')^{68}Ni* reaction. Both reactions have been performed at 50A MeV. For all these predictions, microscopic RPA transition densities are used to calculate the angular distribution.

Fig. 1 shows that the maximum cross section for each reaction is reached below $\theta_{CM} = 8^\circ$, which corresponds to very low energies of the recoiling alpha particle or the recoiling deuteron particle. In order to measure an excitation-energy spectrum from 0 to 30 MeV and between 0° and 8° in the center-of-mass (c.m.) frame, it is necessary to detect alpha particles between 300 keV and 4 MeV at angles from 0° to 90° in the laboratory frame for the ^{68}Ni(α,α')^{68}Ni* reaction, and deuterons between 400 keV and 3 MeV at angles from 0° to 90° in the laboratory frame for the ^{68}Ni(d,d')^{68}Ni* reaction.

Considering an exotic beam with a low production rate and the fact that recoiling particles have as low as a few hundred keV energy, this experiment cannot be performed with a standard setup composed of a solid target and recoiling-particle telescopes. This challenging experiment has been made possible using an active target, where the gas inside is both the target and the detection gas providing both a low-energy detection threshold and a reasonable thickness simultaneously.

The active target MAYA [24] developed at GANIL (Fig. 2) is a time projection chamber (TPC), which has an active volume of $28 \times 25 \times 20\,\mathrm{cm}^3$ filled with the gas used as a target, i.e. He gas at 500 mbar (with 5% of CF_4 as a quencher) for the ^{68}Ni(α,α')^{68}Ni* reaction and D_2 at 1 bar for the ^{68}Ni(d,d')^{68}Ni* reaction. The pressure was adjusted for each reaction in order to detect the recoiling particles up to 8° in the c.m. frame. Both the incoming and scattered ^{68}Ni* and, the scattered alpha particle or deuteron, ionize the gas along their trajectory inside MAYA. The potential difference between the Frisch grid and the top of the detector (cathode) allows the electrons coming from the ionization to drift towards the Frisch grid. Another high voltage is set on the anode which consists of 32 wires placed below the grid. The avalanches on the wires induce a signal on a matrix of 32×32 hexagonal pads connected to GASSIPLEX chips [24]. The pad plane thus provides a two-dimensional projection of the trajectories of the incoming and outgoing particles involved in the reaction. To determine the reaction plane, i.e. the third dimension, the arrival time of the electrons on the wires is registered for each wire. All the high voltage values used for each studied reaction are given in Fig. 2. The energies deposited by the beam and the recoiling alpha or deuteron particles were equivalent in both reactions. However, the nature of the gas and the pressure conditions allow to have a better amplification in the mixture He+CF_4 compared to D_2. Therefore, in the ^{68}Ni(α,α')^{68}Ni* experiment, an electrostatic mask [25] was placed 1 cm below the beam in MAYA to absorb the electrons resulting from the ionization of the gas by the ^{68}Ni beam. This device reduces the amount of electrons collected on the central wires due to the ionization by the ^{68}Ni beam particles and thus increases the sensitivity to the recoiling alpha particle, avoiding saturation of the GASSIPLEX. In the second part of the experiment ^{68}Ni(d,d'), the amplification was weaker and the mask was not required.

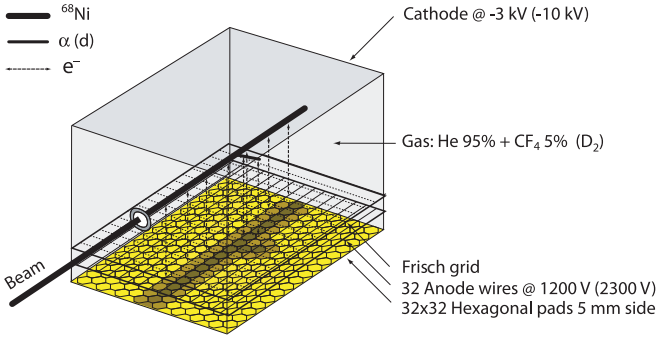

FIG. 2. (Color online) Experimental setup: the active target MAYA used to study both ^{68}Ni(α,α')^{68}Ni* and ^{68}Ni(d,d')^{68}Ni* reactions.

B. Missing-mass analysis

1. *Reconstruction of the range and the scattering angle θ of the reaction in the laboratory frame*

The reconstruction of the range of the recoiling particle, α or d, and of the scattering angle θ follows several steps :

1. The trajectory of the ^{68}Ni* scattered nucleus is reconstructed using the *global fitting method* described in Ref. [26] (due to the beam energy and the position resolution, incoming ^{68}Ni and scattered ^{68}Ni trajectories are not distinguishable). A straight-line trajectory is determined by minimizing the orthogonal distance of the center of the pads weighted by their charge to the line.

2. A "typical" beam track is subtracted from each event. This "typical" beam track corresponds to an average of all the beam tracks observed when there was no reaction in the chamber. This subtraction allows to isolate the recoiling particle track.

3. The fit of the trajectory of the recoiling particle on the pad plane is performed in two steps. Taking only into account the pads with a charge higher than 80% of the maximum charge, a first fit is done using the *global fitting method*. In the second step, for each pad with a non-zero charge, the distance between the pad and the trajectory resulting from the first fit is calculated. If the distance is smaller than two times the mean distance, calculated considering the pads taken into account for the first fit, the pad is taken into account for the second fit. The second fit is done with the selected pads using the same *global fitting method*. It should be noted that a minimum of five pads with a non-zero charge are required for the final fit.

4. These three first steps yield the scattering angle θ_{2D} projected on the pad plane. Events with θ_{2D}

between +10° and +95° on the left side of MAYA, and between −10° and −95° on the right side of MAYA have been selected. This cut allows to focus on elastic and inelastic scattering events, and rejects tracks which are too close to the beam.

5. The three first steps also yield the vertex position of the reaction on the pad plane. Events with a vertex within 3.5 cm of the entrance or exit of MAYA have been rejected. This effectively removes reactions occurring in the entrance window and avoid drift field inhomogeneities due to the presence of silicon detectors.

6. The charges induced on the pads are projected along the recoiling particle trajectory, allowing to deduce the position of the Bragg peak projected on the pad plane. It should be noted that the projection of the charges is done in the direction of the most perpendicular axis of the pad with respect to the trajectory [26].

7. Finally using the time on each wire, the third dimension is reconstructed. Only particles that stopped in the active volume of MAYA have been selected.

Finally, the range of the recoiling particle as well as the scattering angle θ are determined event by event. In the case of the ^{68}Ni(α,α')^{68}Ni* reaction, the extracted range as a function of the total charge deposited for a track allows to select the recoiling α particle and to remove tracks due to reactions on C or on F nuclei. However, in the case of the ^{68}Ni(d,d')^{68}Ni* reaction, the resolution was not sufficient to distinguish deuterons coming from the inelastic scattering, from protons arising from deuteron breakup (see section IV A).

2. *Reconstruction of the excitation energy of ^{68}Ni* and of the scattering angle θ_{CM} in the c.m. frame*

The energy of the recoiling alpha particle (or deuteron) is deduced from its range in the gas using SRIM tables [27]. The feasibility of the trajectory reconstruction depends on the number of pads fired, which sets a threshold of 600 keV for the detection of the recoiling alpha, and 500 keV for the deuteron. Fig. 3 displays the kinematics obtained for both the ^{68}Ni(α,α')^{68}Ni* and the ^{68}Ni(d,d')^{68}Ni* reactions.

Data are then transposed to the c.m. frame using two-body kinematics before being corrected for efficiency. The ACTARsim package was used to evaluate the efficiency. This simulation was developed for the future active target ACTAR and validated using comparisons between simulated and experimental data [28]. One thousand events were simulated per 1 MeV steps in excitation energy of ^{68}Ni* and per 1° steps in angle in the c.m. frame. They were then subjected to the same analysis as the one used for physical events. A matrix of efficiency as

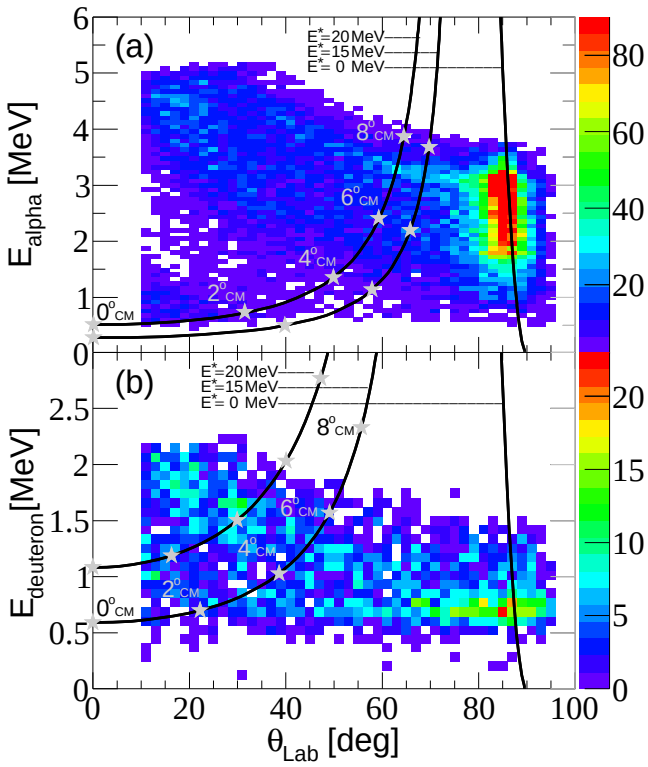

FIG. 3. (Color online) (a) Scatter plot of recoiling alpha energy versus scattering angle in the laboratory frame for the ^{68}Ni(α,α')^{68}Ni* reaction. (b) Same for recoiling deuterons for the ^{68}Ni(d,d')^{68}Ni* reaction.

a function of the angle in the c.m. and of the excitation energy of ^{68}Ni* is obtained and is used to correct the experimental data. This efficiency calculation includes both geometrical and reconstruction efficiency. It evolves from 10% at low angles in the c.m frame ($\theta_{CM} = 1°$), that corresponds to short tracks, to 60% at larger angles in the c.m. ($\theta_{CM} = 6 - 7°$), that corresponds to long tracks. Fig. 4 displays the reconstructed physical events, corrected for efficiency, as a function of the angle in the c.m. frame and the excitation energy of ^{68}Ni*. Due to different pressure conditions, the angular coverage in the c.m. frame and the covered range in excitation energy of ^{68}Ni* are different for the two experiments (Fig. 4 (a) and (b)).

Two independent analyses were then performed for each reaction. In the first one, reconstructed events are projected on the x axis in slices of $1°_{CM}$, and each excitation-energy spectrum is fitted with several contributions with Lorentzian shape and a background. This method is called the fitting method. In the second one, events are projected on the y axis in 2 MeV slices, and each angular distribution is fitted with a background and a linear combination of predicted angular distributions for different multipolarities. This method is called the multipole-decomposition analysis (MDA).

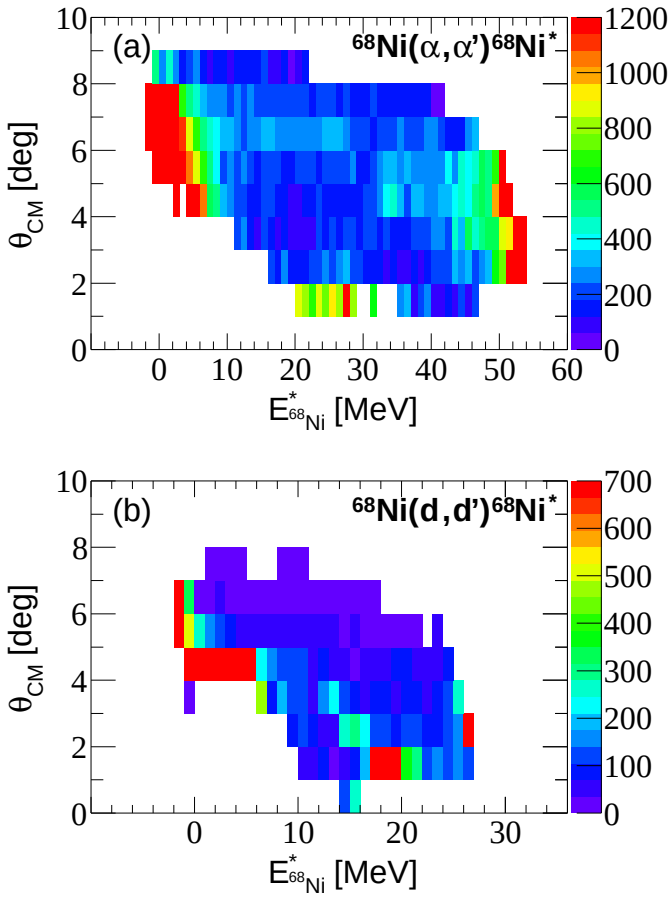

FIG. 4. (Color online) (a) Reconstructed events transformed in the c.m. frame and corrected for geometrical an reconstruction efficiency for the ^{68}Ni(α,α')^{68}Ni* reaction. (b) Same for the ^{68}Ni(d,d')^{68}Ni* reaction.

III. (α,α') RESULTS

From decades of studies on stable nuclei, (α,α') is known as the best probe for measuring ISGR, as both the spin and the isospin of the transition are equal to 0 for this probe [1]. In inverse kinematics, with an active target, an additional difficulty arises, i.e. the He gas requires a quencher in order to serve as a detection gas in the active target, so the target is no longer pure (He with 5% of CF_4). The other difficulty is the necessity of masking the beam, as explained in section II.

A. Background

The origin of the background in inelastic scattering remains somewhat puzzling [1], but is generally considered as a mixture of contributions from the knock-out processes, overlapping resonances, multi-step processes and high multipolarity states. It has been described by many different shapes over the years. We decided to use the simplest shape, a flat background, and to set the height of the background at the maximum value compatible with the data, i.e. the minimum of the spectrum between 12 and 30 MeV for each angle in the c.m. frame. In this way, the background may be overestimated and physical events may be lost. For example, the angular distribution of this background will follow a monopole shape at small angles in the c.m. frame. However, this method ensures that the data above this background are of physical origin.

B. Fitting analysis

The excitation-energy spectrum of ^{68}Ni obtained for the ^{68}Ni(α,α')^{68}Ni* reaction and corrected for efficiency is displayed in Fig. 5 (a). A fit of the elastic scattering peak gives a 2 MeV FWHM resolution, which is an upper limit since the first-excited states are included in this peak. A zoom in the region of ISGR (Fig. 5 (b)) shows different structures whose intensities depend on the c.m. angle. The excitation-energy spectrum obtained at each angle in the c.m. has been fitted with a linear combination of the flat background described above and four resonances corresponding to the observed peaks around 13 MeV, 16 MeV, 21 MeV and 26 MeV. Fig. 5 displays the result of the fit of the excitation-energy spectrum for all angles (b) and at each angle in the c.m. frame ((c) to (g)).

Three resonances have been identified with this method, and their centroids are given in Table I. Error bars are based on the dispersion of the extracted centroids at each angle in the c.m. frame. The additional resonance around 26 MeV is most probably a combination of $L = 0, 1, 3$ multipolarities, as already observed in this mass region for stable isotopes [1, 30]. Considering the present statistics, it is not relevant to try to extract the individual contributions to this structure.

	^{68}Ni(α,α')^{68}Ni*	^{68}Ni(d,d')^{68}Ni*
Resonance 1	12.9 ± 1.0	12.6 ± 0.3
Resonance 2	15.9 ± 1.3	15.4 ± 1.6
Resonance 3	21.1 ± 1.9	20.8 ± 0.6

TABLE I. Centroid of the resonances measured in the ^{68}Ni(α,α')^{68}Ni* experiment (left column) and in the ^{68}Ni(d,d')^{68}Ni* experiment (right column). These resonances have been obtained by fitting the excitation-energy spectra shown in Fig. 5 and Fig. 10.

For a given resonance, studying the evolution of the peak intensity as a function of the c.m. angle, provides its angular distribution. We have fitted the angular distribution of the resonance at 12.9 MeV with different multipolarities, the resonance at 15.9 MeV assuming an $L = 2$ multipolarity, and the resonance at 21.1 MeV assuming

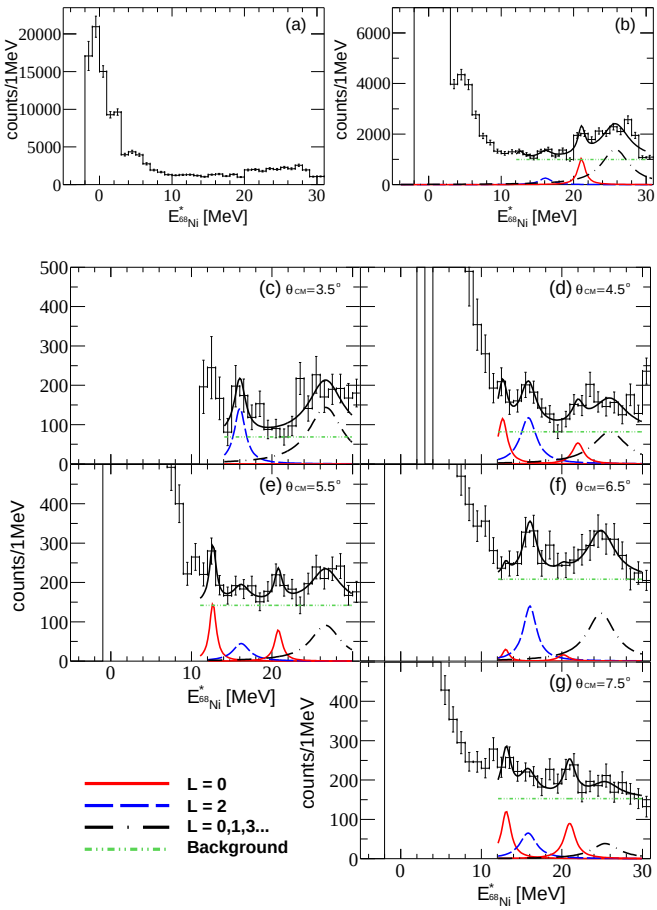

FIG. 5. (Color online) (a) Excitation-energy spectrum of ^{68}Ni obtained for the ^{68}Ni(α,α')^{68}Ni* reaction, for all angles deduced from the alpha kinematics and corrected for efficiency. (b) Same with a zoom on the ISGR region. The background is represented with a green dot-dot-short-dashed line. The fitted resonances which are expected to be of monopole character are represented with a red solid line, and the one that is expected to be of quadrupole character is represented in blue long-dashed line. The resonance at higher energy, composed of several multipolarities $L = 0, 1, 3$, is represented in black dot-long-dashed line. The solid black line corresponds to the sum of all contributions. From (c) to (g) the same at $\theta_{CM} = 3.5°$, $4.5°$, $5.5°$, $6.5°$, $7.5°$. In (c) and (d) there is no data at low energy due to geometrical acceptance as shown in Figure 4 (a).

an $L = 0$ multipolarity (Fig. 6). The fits were performed using the DWBA predictions (Fig. 1) of the model described at the beginning of section II. In Fig. 6 (a1) the angular distribution of the resonance at 12.9 MeV is well described by the shape of an $L = 0$ prediction. However, the angular range covered in this experiment, [$\theta_{CM} = 4.5°$, $\theta_{CM} = 8.5°$], is less characteristic than at lower angles, and it is difficult to reject an $L = 1$ (Fig. 6 (a2)) or $L = 2$ (Fig. 6 (a3)) nature of the resonance. In Fig. 6 (b), fitting the angular distribution of the reso-

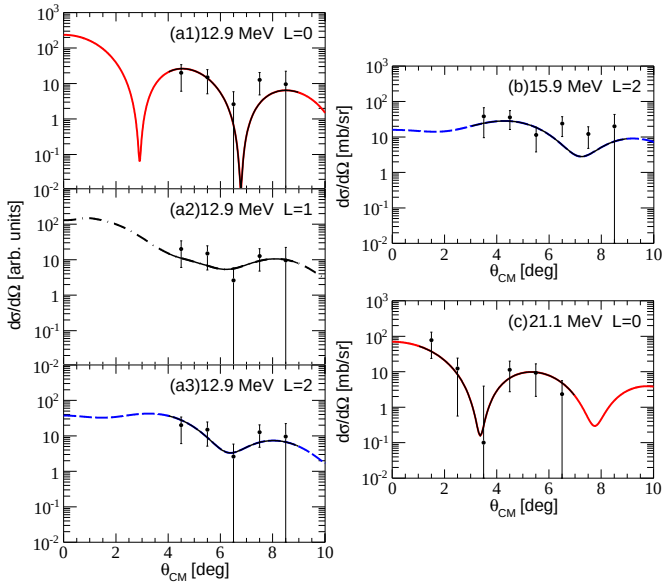

FIG. 6. (Color online) (a) Experimental angular distribution extracted for the resonance at 12.9 MeV and fitted assuming an $L = 0$ multipolarity (a1), $L = 1$ multipolarity (a2), or $L = 2$ multipolarity (a3). (b) The same for the resonance at 15.9 MeV assuming an $L = 2$ multipolarity. (c) The same for the resonance at 21.1 MeV assuming an $L = 0$ multipolarity.

nance located at 15.9 MeV with an $L = 2$ multipolarity seems reasonable, but this has to be confirmed with the MDA analysis since the angular distribution of an $L = 2$ resonance is not as characteristic as the one of an $L = 0$ resonance. The angular distribution for the resonance at 21.1 MeV (Fig. 6 (c)) is well described assuming an $L = 0$ multipolarity. It should be noted that this 21.1 MeV resonance only corresponds to the first part of the ISGMR, considering the whole ISGMR involves both this resonance at 21.1 MeV and the $L = 0$ strength in the large bump around 26 MeV. However, as mentioned above, the 26 MeV bump is not relevant for a detailed analysis, given the present uncertainties.

C. MDA

For each bin of 2 MeV of ^{68}Ni excitation energy, the angular distribution is fitted by a linear combination of theoretical angular distributions of $L = 0, 1, 2$ multipolarities and the flat background described above. Fig. 7 displays this analysis for each slice between 10 and 24 MeV.

In the [20 MeV,22 MeV] slice, the $L = 0$ multipolarity dominates, confirming the nature of the resonance observed at 21.1 MeV in the fitting method. In Fig. 7 (d) (16 to 18 MeV energy slice), there is some $L = 2$ strength which is not observed in Fig. 7 (c) (from 14 to 16 MeV) or in Fig. 7 (e) (from 18 to 20 MeV), indicating that the

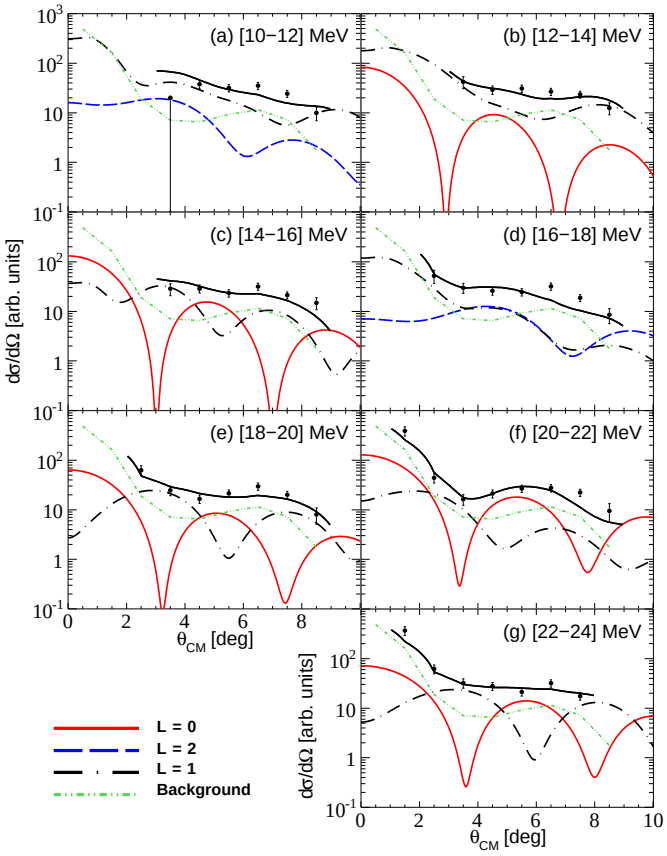

FIG. 7. (Color online) (a) Experimental ^{68}Ni angular distribution extracted in 2 MeV broad bins of excitation energy and fitted with a linear combination of $L = 0, 1, 2$ theoretical angular distributions and a background. The solid black line corresponds to the sum of all contributions.

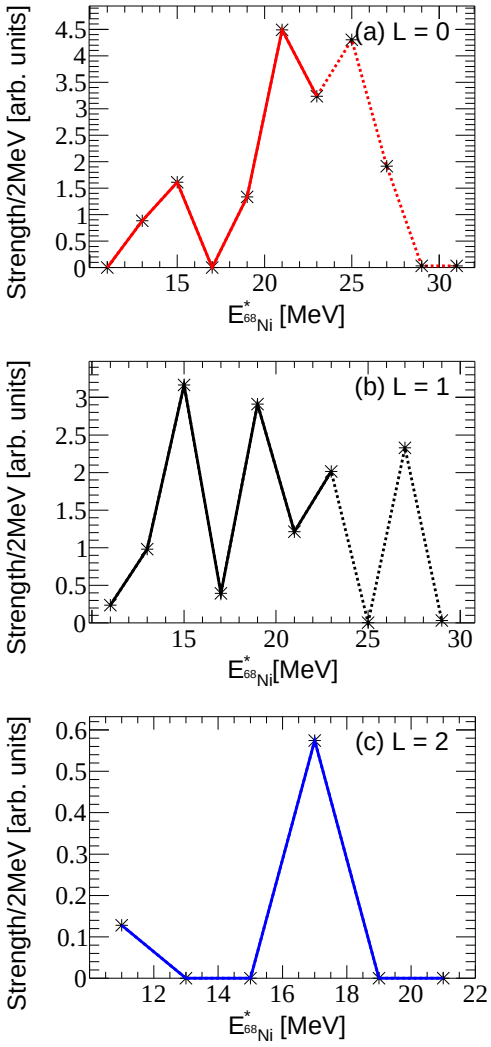

FIG. 8. (Color online) (a) Monopole strength distribution in ^{68}Ni resulting from MDA. (b) Same for dipole strength. (c) Same for quadrupole strength.

$L = 2$ strength is localized around 17 MeV of excitation energy of ^{68}Ni, in agreement with the fitting analysis. In the [12 MeV,16 MeV] region the fit gives $L = 0$ and $L = 1$ contributions of similar amplitudes.

The energy dependence of the magnitude extracted from the fit for a given multipolarity gives access to the strength distribution for this multipolarity. Fig. 8 displays this strength distribution for $L = 0$ (a), $L = 1$ (b) and $L = 2$ (c). Due to large error bars coming from difficulties to measure the beam intensity, and from the possible background overestimation, absolute exhausted percentage of energy-weighted sum rules could not be extracted.

Fig. 8 (a) shows that the ISGMR is located between 19 MeV and 27 MeV, with a mean energy at 23.4 MeV, given by m_1/m_0 where m_1 is the moment of order 1 and m_0 the moment of order 0. The shape is spread as expected and a fragment is clearly observed at 21 MeV in agreement with the result of the fitting method which already allowed identifying this first part of the ISGMR.

The higher energy part cannot be identified with the same accuracy, due to its mixing with larger multipolarities components. It is, therefore, difficult to estimate the total width of the ISGMR. An increase of the strength around 14 MeV is observed, with a similar increase in the case of the $L = 1$ multipolarity (Fig. 8 (b)). This observation, already made in discussion Fig. 7 (a, b and c) shows that the resonance observed at 12.9 MeV with the fitting method could be a superposition of the soft isoscalar monopole mode and isoscalar dipole strength. The resolution of the present setup does not allow to separate these two contributions. In the case of the $L = 2$ multipolarity, the MDA shows that there is a concentration of quadrupole strength around 17 MeV (Fig. 8 (c)), confirming that the resonance observed at 15.9 MeV in the fitting method is in part composed of the ISGQR.

The complementary contribution, in equivalent proportion, is the ISGDR, as shown in Fig. 7 (d).

IV. (d,d') RESULTS

Using a deuteron probe in inverse kinematics has advantages. The first advantage is that the first minimum of the $L = 0$ angular distribution is located at an angle larger than for the inelastic alpha scattering case (Fig. 1), i.e. 7°_{CM} instead of 3°_{CM}. Another advantage is that neither a quencher (so D_2 is a pure target) nor a beam mask is required. The drawback of this probe is that a deuteron breakup background is expected. It is, therefore, relevant to compare the quality of the results obtained by inelastic deuteron scattering, with those from inelastic alpha scattering described previously.

A. Background

In the ^{68}Ni(d,d')^{68}Ni* reaction, the background is dominated by deuteron breakup [14]. Indeed, considering the charge resolution, it was not possible to distinguish scattered deuterons from inelastic scattering ^{68}Ni(d,d') and protons from deuteron breakup ^{68}Ni(d,p). We have, therefore, used the experimental cross section of deuteron breakup on ^{58}Ni in direct kinematics at 50A MeV [29] to simulate and estimate this background. First, protons are generated in direct kinematics, following the experimental cross section, using a Monte Carlo simulation. In a second step, these simulated events are transformed from the direct to the inverse kinematics frame and then to the c.m. frame. Finally, this deuteron breakup distribution is corrected for efficiency, including geometrical and reconstruction efficiency as described in section II. Fig. 9 displays the simulated proton distribution coming from the deuteron breakup as a function of the angle in the c.m. and the excitation energy of ^{68}Ni.

The breakup contribution is maximum around an excitation energy of 10 MeV and around 5°_{CM}, which is not the region of interest for isoscalar giant resonances. This breakup background is normalized to the data, by maximizing its contribution without exceeding the physical data. It should be noted that since the deuteron breakup angular distribution is known, only one normalization factor, obtained at 6.5°_{CM} where the breakup background fits the experimental data, was necessary.

B. Fitting analysis

The fitting methods described for the ^{68}Ni(α,α')^{68}Ni* reaction have been applied in the same way to the ^{68}Ni(d,d')^{68}Ni* reaction. Fig. 10 (a) displays the global excitation-energy spectrum corrected for efficiency and fitted with a linear combination of several resonances and the simulated background. The fit of the elastic peak gives a resolution around 3 MeV FWHM and for the same reason as for the ^{68}Ni(α,α')^{68}Ni* experiment, it is only an upper limit. Because of the smaller acceptance in excitation energy for the ^{68}Ni(d,d')^{68}Ni* reaction, we distinguish only three structures instead of the four observed in Fig. 5, the large structure around 26 MeV is missing. The excitation-energy spectrum has also been fitted in the same way at different angles of 2.5°, 3.5°, 4.5° and 5.5° in the c.m. frame (Figs. 10 (b) to (e)).

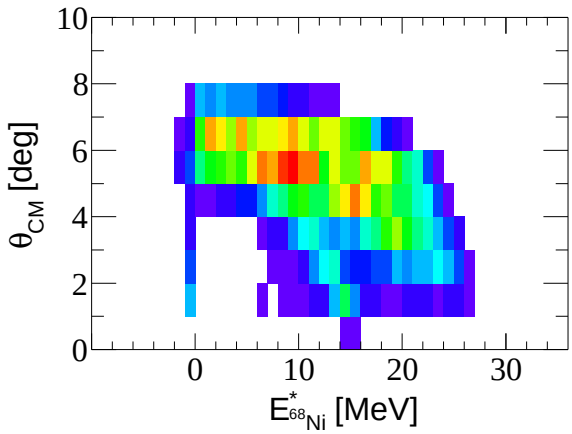

FIG. 9. (Color online) Proton distribution coming from the deuteron breakup on ^{68}Ni, corrected for efficiency.

Three resonances are identified at 12.6, 15.4, and 20.8 MeV (Table I). In the same way as in section III.B, one can evaluate the multipolarity of each resonance by studying the evolution of its area as a function of the angle in the c.m. frame. The resonance at 12.6 MeV and the one at 20.8 MeV are fitted in Fig. 11 assuming an $L = 0$ multipolarity (DWBA), and the resonance at 15.4 MeV with an $L = 2$ multipolarity. The angular distribution for the resonance at 15.4 MeV is not presented because the fit is not conclusive, since all the points are associated with large errors bars and are almost compatible with zero. Due to the flat behavior of the $L = 2$ angular distribution (Fig. 1), it is not possible to disentangle it from the background. It has been concluded that the ^{68}Ni(d,d')^{68}Ni* experiment is not sensitive to the ISGQR. More generally, because of the low statistics and the small angular coverage, it is difficult to draw strong conclusions in the case of the (d,d') results, but the angular distributions for both the resonances at 12.6 MeV and at 20.8 MeV match the $L = 0$ shape, in agreement with the (α,α') results.

C. MDA

The MDA has also been performed in the case of the ^{68}Ni(d,d')^{68}Ni* data. The fit of the angular distribution for each slice of 2 MeV of excitation energy has been per-

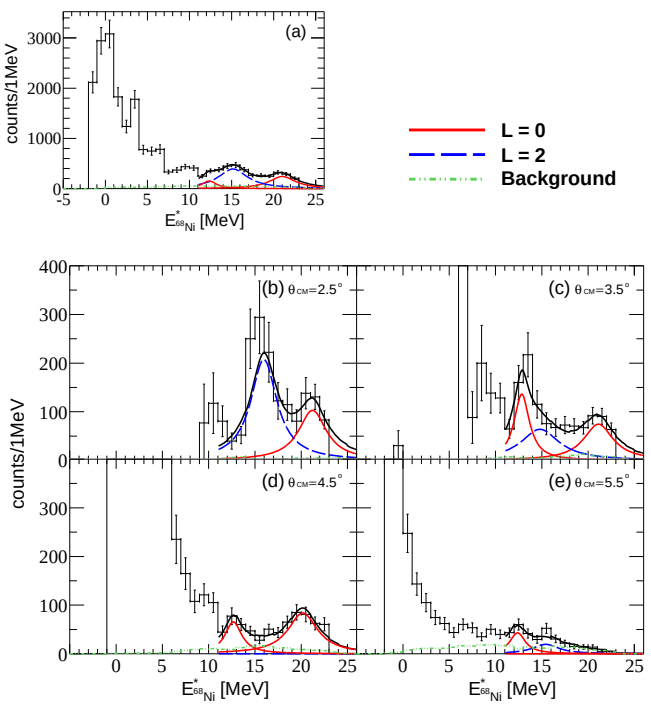

FIG. 10. (Color online) (a) Excitation-energy spectrum of ^{68}Ni obtained in the ^{68}Ni(d,d')^{68}Ni* reaction, for all angles deduced from the deuteron kinematics and corrected for efficiency. The subtracted background is represented with a green dot-dot-short-dashed line. The resonances resulting from the fits are represented with a red solid line ($L = 0$), and with a blue long-dashed line ($L = 2$). The solid black line corresponds to the sum of all contributions. Figs. (b) to (e) show the same fit at different angles in the c.m. frame, from 2.5° to 5.5°.

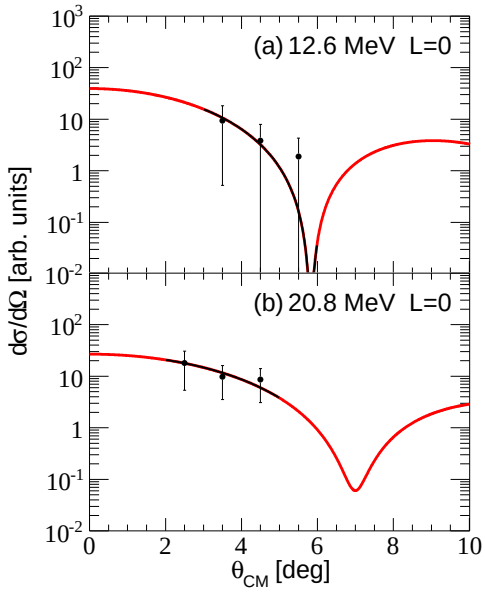

FIG. 11. (Color online) (a) Experimental angular distribution extracted for the resonance at 12.6 MeV and fitted assuming an $L = 0$ multipolarity. (b) The same for the resonance at 20.8 MeV.

formed with a linear combination of the breakup background, an $L = 0$ and an $L = 2$ contribution. This experiment is not sensitive enough to add an $L = 1$ multipolarity, unlike in the ^{68}Ni(α,α')^{68}Ni* experiment. Fig. 12 displays the MDA for all the slices of 2 MeV wide between 10 and 24 MeV. Over the full range of excitation energy, the $L = 2$ contribution is negligible compared to the $L = 0$, confirming what has been observed in the fitting method. At low energies, especially around 11 MeV, the data points are not well fitted, possibly due to the presence of $L = 1$ strength in this region which is not taken into account.

Fig. 13 displays the monopole strength of ^{68}Ni obtained from the ^{68}Ni(d,d')^{68}Ni* reaction. Even if this analysis is not straightforward, an increase of the isoscalar monopole strength around 21 MeV emerges which confirms the observations of the ^{68}Ni(α,α')^{68}Ni* experiment, and the results of the fitting method for ^{68}Ni(d,d')^{68}Ni*. It can also be noted that there is a weak broad structure between 14 and 18 MeV, in the same region where the soft isoscalar monopole mode is observed in the ^{68}Ni(α,α')^{68}Ni* experiment.

V. DISCUSSION

The ISGR in ^{68}Ni have been measured through two inelastic scattering reactions ^{68}Ni(α,α')^{68}Ni* and ^{68}Ni(d,d')^{68}Ni* using the active target MAYA as a detector. The active target MAYA was successfully used with a mixture of (He+CF_4) to measure the inelastic α scattering, and with D_2 to measure inelastic deuteron scattering, both in inverse kinematics. The statistics were higher for the α-scattering measurement than for the deuteron-scattering measurement. This is explained by a larger cross section, and mainly by the pressure and high voltage conditions used, allowing for a better amplification in (α,α') than in (d,d'). The statistics in the ^{68}Ni(d,d')^{68}Ni* experiment, the angular and excitation-energy coverage and resolution are too limited to provide conclusive results. As a consequence, the ^{68}Ni(d,d')^{68}Ni* is considered here more as a cross check of what has been observed in the ^{68}Ni(α,α')^{68}Ni* experiment, than as an independent analysis. The final results on the ISGR in ^{68}Ni are deduced from the analysis of ^{68}Ni(α,α')^{68}Ni* scattering experiment.

The two complementary analyses, the fitting method and the MDA, in the ^{68}Ni(α,α')^{68}Ni* experiment allow to identify ISGMR strength. The dominant component is observed at 21.1 MeV, and the $L = 0$ multipolarity is clearly identified both from the angular distribution of the fitted peak and in MDA. This result has been confirmed by the ^{68}Ni(d,d')^{68}Ni* experiment. The ISGQR is measured at 15.9 MeV by the fitting method. However, it seems to be mixed with ISGDR strength, so that it is

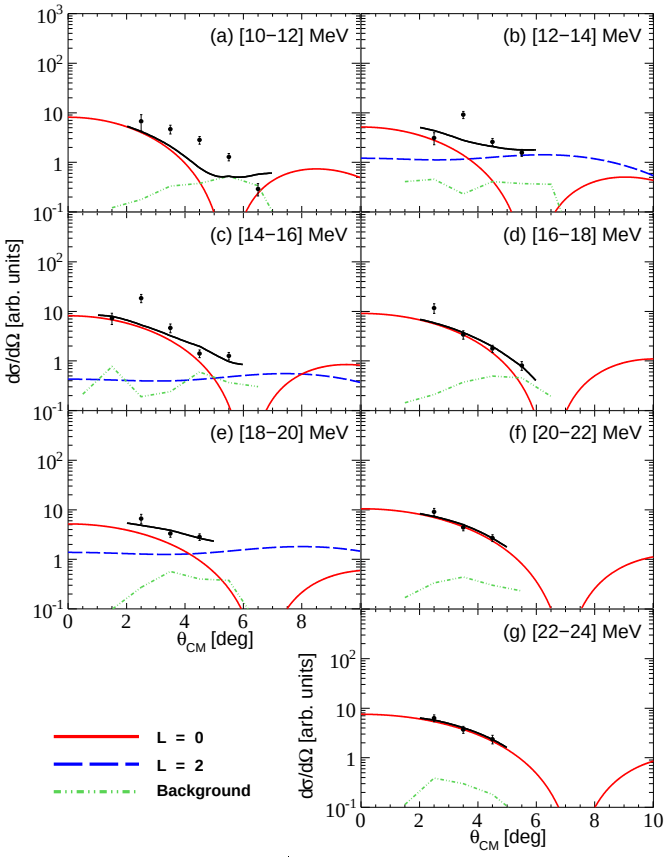

FIG. 12. (Color online) Experimental ^{68}Ni angular distribution extracted for 2 MeV bins of excitation energy and fitted with a linear combination of $L = 0$ and $L = 2$ theoretical angular distributions and the simulated deuteron breakup induced background. The solid black line corresponds to the sum of all contributions.

possible that the evaluated error bar of 1.3 MeV on its centroid is underestimated. The ISGQR is not observed in the ^{68}Ni(d,d')^{68}Ni* experiment. It should be noted that the shape of the angular distribution is less characteristic for the ISGQR than that for the ISGMR, which makes its separation from the background and the multipolarity assignment less certain than for the ISGMR. A possible indication of a soft isoscalar monopole resonance is found at 12.9 ± 1.0 MeV, in the fitting method in ^{68}Ni(α,α')^{68}Ni* reaction. The presence of $L = 0$ strength in this energy region is confirmed by the MDA in the ^{68}Ni(α,α')^{68}Ni* and ^{68}Ni(d,d')^{68}Ni* experiments. However, the MDA in ^{68}Ni(α,α')^{68}Ni* also shows that isoscalar dipole strength is mixed with the soft monopole in this energy region. It is the first time that indications of the ISGDR are observed in an unstable nucleus. MDA in ^{68}Ni(α,α')^{68}Ni* yields some isoscalar dipole strength around 15 MeV and between 18 MeV and 24 MeV. This is reasonable according to the large spreading of isoscalar dipole strength predicted in reference [10]. Following the

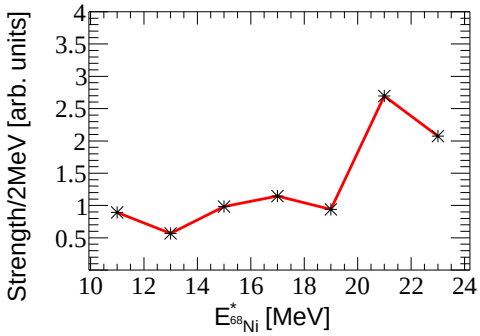

FIG. 13. (Color online) Monopole strength distribution resulting from MDA.

one presented in this paper, a dedicated experiment to measure the ISGDR in an unstable nucleus (^{56}Ni) has been performed at GANIL with the same setup [31]. Table II presents a comparison between the results of the two present experiments and the other results for the Ni isotopic chain.

In Ref. [30] presented in Table II, the ISGDR in ^{58}Ni and in ^{60}Ni is found fragmented, whereas the ISGQR is well fitted with a Gaussian function. These two typical shapes for ISGDR and ISGQR are also observed in our ^{68}Ni experiment. In the same reference, the ISGMR is observed with a tail at high energy in ^{58}Ni and ^{60}Ni. This asymmetry of the ISGMR is typical of nuclei in this mass region but the ISGMR measured here in ^{68}Ni is more fragmented than what is observed for stable nuclei. In addition, the centroid of this ISGMR in ^{68}Ni is located at higher energy than what is expected along the Ni isotopic chain, but also associated with large error bars.

The widths derived from the fitting method for the ^{68}Ni(α,α')^{68}Ni* experiment are extracted with large uncertainties. This is mainly due to the evaluation of the background, and to a lesser extent to the limited statistics. As the background is maximized in order to make sure that the background subtracted data obtained above are really physical, the widths of the resonances are artificially decreased. Widths are less straightforward to extract than centroids and this is a clear limitation of the technique used in this experiment.

More generally, the present experiment lies at the limit of what is possible to study in ISGR with this setup. In ^{68}Ni, the isoscalar monopole and dipole strengths are much more fragmented than in stable nuclei. Due to the present excitation energy resolution, resonances in the same region overlap and it becomes delicate to separate their contributions using the fitting method. Moreover, the use of MDA raises a significant issue, i.e. how to analyze the strength in an energy region where RPA transition densities for the soft modes are not predicted, in contrast to the Giant Resonance case?

		^{56}Ni	^{58}Ni		^{60}Ni	^{62}Ni	^{64}Ni	^{68}Ni	
		^{56}Ni(d,d')^{56}Ni*	^{58}Ni(α,α')^{58}Ni*		^{60}Ni(α,α')^{60}Ni*	^{62}Ni(α,α')^{62}Ni*	^{64}Ni(α,α')^{64}Ni*	^{68}Ni(α,α')^{68}Ni*	^{68}Ni(d,d')^{68}Ni*
		[14]	[30]	[32]	[30]	[33]	[33]	This work	
soft ISGMR	E_c (MeV)							Fit$^{\diamond\diamond}$ 12.9 ± 1.0	Fit 12.6 ± 0.3
	E_c (MeV)							MDA 14.3 ± 0.5	
ISGMR	E_c (MeV)	Fit 19.5	Fit 18.43 ± 0.15		Fit 17.62 ± 0.15			Fit 21.1 ± 1.9	Fit 20.8 ± 0.6
	EWSR (%)		82^{+11}_{-9}		67^{+12}_{-9}				
	E_c (MeV)	MDA 19.3 ± 0.5	MDA $19.20^{+0.44}_{-0.19}$	MDA $19.9^{+0.7}_{-0.8}$	MDA $18.04^{+0.35}_{-0.23}$			MDA 23.4 ± 1.4	
	EWSR (%)	136 ± 27	85^{+13}_{-10}	92^{+4}_{-3}	82^{+13}_{-11}				
ISGDR	E_c (MeV)		Fit 17.42 ± 0.25		Fit 16.01 ± 0.20			Fit$^{\diamond\diamond}$ 12.9 ± 1.0	
peak 1	EWSR (%)		4 ± 2		6 ± 3				
ISGDR	E_c (MeV)		Fit 34.06 ± 0.30		Fit $36.11^{+0.29}_{-0.27}$			MDA$^{\diamond}$ 20.7 ± 0.6	
peak 2	EWSR (%)		86 ± 12		120 ± 16				
	E_c (MeV)		MDA$^{\diamond}$ $27.78^{+0.47}_{-0.30}$	MDA $30.8^{+1.7}_{-1.1}$	MDA$^{\diamond}$ 24.93 ± 0.46				
	EWSR (%)		68^{+20}_{-15}	98^{+4}_{-5}	72 ± 17				
ISGQR	E_c (MeV)	Fit 16.5	Fit 16.64 ± 0.12		Fit 16.05 ± 0.12	Fit 15.81 ± 0.40	Fit 15.60 ± 0.30	Fit 15.9 ± 1.3	Fit 15.4 ± 1.6
	EWSR (%)		81 ± 10		71 ± 10	78 ± 14	90 ± 16		
	E_c (MeV)	MDA 16.2 ± 0.5	MDA $16.31^{+0.17}_{-0.10}$	MDA $16.3^{+0.8}_{-0.9}$	MDA $15.84^{+0.18}_{-0.10}$			MDA 17 ± 1.0	
	EWSR (%)	76 ± 13	82 ± 10	73 ± 3	71 ± 10				

TABLE II. (Color online) Soft ISGMR, ISGMR, ISGDR and ISGQR centroids and EWSR measured along the Ni isotopic chain. The unstable nuclei are highlighted in gray, corresponding to reactions studied in inverse kinematics with the active target MAYA. $^{\diamond}$This MDA includes peak 1 and peak 2 of reference [30] and the full [11-29 MeV] range without distinction of peak 1 and 2 for the present experiment. $^{\diamond\diamond}$This resonance mixes $L = 0$ and $L = 1$ contributions.

VI. CONCLUSION

We have studied the ISGR for the first time in the unstable neutron-rich nucleus ^{68}Ni. This work has been performed by studying the two inelastic scattering reactions ^{68}Ni(α,α')^{68}Ni* and ^{68}Ni(d,d')^{68}Ni* in inverse kinematics, and using a dedicated detector, the active target MAYA. The ISGMR has been found fragmented with a fragment clearly identified in both reactions at 21.1 MeV. The ISGQR has been measured only in the ^{68}Ni(α,α')^{68}Ni* experiment at 15.9 MeV. For the first time, a possible indication of a soft monopole mode around 13-14 MeV and of an isoscalar dipole strength in the same region has been obtained as well as isoscalar dipole strength in the 18-24 MeV region. These are promising results for the physics of ISGR in exotic nuclei.

Several issues owing to the limitation of the detection setup for low-energy recoiling particles have been raised, i.e. the energy and angle resolutions, recoiling particle trajectories close to the beam trajectory, the complex strength distribution pattern expected in exotic nuclei and the extraction of resonance widths. This points towards the necessity of an upgrade of active-target setups, as well as alternative methods such as storage ring with windowless gas-jet target and detector telescopes [34]. The next generation of active targets, based on more recent technologies like gas electrons multiplier (GEM) [35] or micro mesh gaseous (MICROMEGAS) detector [36], and associated with high granularity pad plane, will permit to increase the efficiency. In particular, a better resolution will be obtained for short tracks, which correspond to small angles in the c.m. frame, where the cross section is higher and the angular distribution is more characteristic for a given multipolarity. So, it will offer a better sensitivity to the different multipolarity contributions. The pad plane will be connected to a new generation electronics, that will allow to connect a large number of channels and have a more selective trigger. Several active targets encompassing such developments are being constructed worldwide [28, 37–39], which promise a bright future for ISGR studies of nuclei far from stability.

Acknowledgments

The authors thank M. Marqués for fruitful discussions. This work has been supported by Institut Universitaire de France and in part by U. S. National science Foundation (Grant No. PHYS-1068192). The research leading to these results has received funding from the European Union's Seventh Framework Programme under grant agreement No. 262010.

[1] M.N. Harakeh and A. van der Woude, *Giant Resonances*, Oxford University Press (2001).
[2] E. Khan, J. Margueron, and I. Vidaña, Phys. Rev. Lett. 109, 092501 (2012).
[3] E. Khan and J. Margueron, Phys. Rev. C 88, 034319 (2013).

[4] L. Capelli, G. Colò, and J. Li, Phys. Rev. C 79, 054329 (2009).

[5] E. Khan, N. Paar, and D. Vretenar, Phys. Rev. C 84, 051301 (2011).

[6] E. Khan, N. Paar, D. Vretenar, Li-Gang Cao, H. Sagawa, and G. Colò, Phys. Rev. C 87, 064311 (2013).

[7] I. Hamamoto and H. Sagawa, Phys. Rev. C 90, 031302 (2014).

[8] M.N. Harakeh, Phys. Lett. B 90, 13 (1980).

[9] M.N. Harakeh and A. E. L. Dieperink, Phys. Rev. C 23, 2329 (1981).

[10] D. Vretenar, Y. F. Niu, N. Paar, and J. Meng, Phys. Rev. C 85, 044317 (2012).

[11] D. Savran, T. Aumann, and A. Zilges, Prog. Part. Nucl. Phys. 70, 210 (2013).

[12] O. Wieland, A. Bracco, F. Camera, G. Benzoni, N. Blasi, S. Brambilla, F. C. L. Crespi, S. Leoni, B. Million, R. Nicolini, A. Maj, P. Bednarczyk, J. Grebosz, M. Kmiecik, W. Meczynski, J. Styczen, T. Aumann, A. Banu, T. Beck, F. Becker, L. Càceres, P. Doornenbal, H. Emling, J. Gerl, H. Geissel, M. Gorska, O. Kavatsyuk, M. Kavatsyuk, I. Kojouharov, N. Kurz, R. Lozeva, N. Saito, T. Saito, H. Schaffner, H. J. Wollersheim, J. Jolie, P. Reiter, N. Warr, G. deAngelis, A. Gadea, D. Napoli, S. Lenzi, S. Lunardi, D. Balabanski, G. LoBianco, C. Petrache, A. Saltarelli, M. Castoldi, A. Zucchiatti, J. Walker, and A. Bürger, Phys. Rev. Lett. 102, 092502 (2009).

[13] D. M. Rossi, P. Adrich, F. Aksouh, H. Alvarez-Pol, T. Aumann, J. Benlliure, M. Böhmer, K. Boretzky, E. Casarejos, M. Chartier, A. Chatillon, D. Cortina-Gil, U. Datta Pramanik, H. Emling, O. Ershova, B. Fernandez-Dominguez, H. Geissel, M. Gorska, M. Heil, H. T. Johansson, A. Junghans, A. Kelic-Heil, O. Kiselev, A. Klimkiewicz, J. V. Kratz, R. Krücken, N. Kurz, M. Labiche, T. Le Bleis, R. Lemmon, Yu. A. Litvinov, K. Mahata, P. Maierbeck, A. Movsesyan, T. Nilsson, C. Nociforo, R. Palit, S. Paschalis, R. Plag, R. Reifarth, D. Savran, H. Scheit, H. Simon, K. Sümmerer, A. Wagner, W. Waluś, H. Weick, and M. Winkler, Phys. Rev. Lett. 111, 242503 (2013).

[14] C. Monrozeau, E. Khan, Y. Blumenfeld, C. E. Demonchy, W. Mittig, P. Roussel-Chomaz, D. Beaumel, M. Caamaño, D. Cortina-Gil, J. P. Ebran, N. Frascaria, U. Garg, M. Gelin, A. Gillibert, D. Gupta, N. Keeley, F. Maréchal, A. Obertelli, and J. A. Scarpaci, Phys. Rev. Lett. 100, 042501 (2008).

[15] M. Vandebrouck, J. Gibelin, E. Khan, N. L. Achouri, H. Baba, D. Beaumel, Y. Blumenfeld, M. Caamaño, L. Càceres, G. Colò, F. Delaunay, B. Fernandez-Dominguez, U. Garg, G. F. Grinyer, M. N. Harakeh, N. Kalantar-Nayestanaki, N. Keeley, W. Mittig, J. Pancin, R. Raabe, T. Roger, P. Roussel-Chomaz, H. Savajols, O. Sorlin, C. Stodel, D. Suzuki, and J. C. Thomas, Phys. Rev. Lett. 113, 032504 (2014).

[16] R. Anne, D. Bazin, A.C. Mueller, J.C Jacmart, and M. Langevin, Nucl. Instr. Meth A257, 215 (1987).

[17] T. Li, U. Garg, Y. Liu, R. Marks, B. K. Nayak, P. V. Madhusudhana Rao, M. Fujiwara, H. Hashimoto, K. Nakanishi, S. Okumura, M. Yosoi, M. Ichikawa, M. Itoh, R. Matsuo, T. Terazono, M. Uchida, Y. Iwao, T. Kawabata, T. Murakami, H. Sakaguchi, S. Terashima, Y. Yasuda, J. Zenihiro, H. Akimune, K. Kawase, and M. N. Harakeh, Phys. Rev. C 81, 034309 (2010).

[18] G. Colò, L. G. Cao, N. Van Giai, L. Capelli, Comp. Phys. Comm. 184, 142 (2013).

[19] P. G. Reinhard and H. Flocard, Nucl. Phys. A584, 467 (1995).

[20] I. J. Thompson, Comput. Phys. Rep. 7, 167 (1988).

[21] J. Cook, Comput. Phys. Commun. 25, 125 (1982).

[22] J. Albiński, C. Alderliesten, J. Bojowald, A. Budzanowski, H. Dabrowski, C. Mayer-Böricke, W. Oelert, H. Rebel, Z. Rogalska, D. K. Srivastava, P. Turek, and S. Wiktor, Nucl. Phys. A 445 477 (1985).

[23] L. Hulthén and M. Sugawara, *The two-nucleon problem*, Springer-Verlag, Berlin (1957).

[24] C.E. Demonchy, W. Mittig, H. Savajols, P. Roussel-Chomaz, M. Chartier, B. Jurado, L. Giot, D. Cortina-Gil, M. Caamaño, G. Ter-Akopian, A. Fomichev, A. Rodin, M.S. Golovkov, S. Stepantsov, A. Gillibert, E. Pollacco, A. Obertelli, and H. Wang, Nucl. Instr. Meth. A573, 145 (2007).

[25] J. Pancin , J. Gibelin, M. Goth, P. Gangnant, J. F. Libin, R. Raabe, T. Roger and P. Roussel-Chomaz, JINST 7, P01006 (2012).

[26] T. Roger, M. Caamaño, C.E. Demonchy, W. Mittig, H. Savajols and I. Tanihata, Nucl. Instr. Meth A638, 134 (2011).

[27] J. F. Ziegler, J. Appl. Phys. 85, 1249 (1999).

[28] J. Pancin, S. Damoy, D. Perez Loureiro, V. Chambert, F. Dorangeville, F. Druillole, G.F. Grinyer, A. Lermitage, A. Maroni, G. Nol, C. Porte, T. Roger, P. Rosier, and L. Suen, Nucl. Instr. Meth A735, 532 (2014).

[29] D. Ridikas, W. Mittig, H. Savajols, P. Roussel-Chomaz, S. V. Förtsch, J. J. Lawrie, and G. F. Steyn, Phys. Rev. C 63, 014610 (2000).

[30] Y.-W. Lui, D. H. Youngblood, H. L. Clark, Y. Tokimoto, and B. John, Phys. Rev. C 73, 014314 (2006).

[31] S. Bagchi, *Study of Compression Modes in ^{56}Ni using an Active Target*, Ph.D. thesis, University of Groningen, The Netherlands (2015).

[32] B. K. Nayak, U. Garg, M. Hedden, M. Koss, T. Li, Y. Liu, P. V. Madhusudhana Rao, S. Zhu, M. Itoh, H. Sakaguchi, H. Takeda, M. Uchida, Y. Yasuda, Y. Yosoi, H. Fujimura, M. Fujiwara, K. Hara, T. Kawabata, H. Akimune and M. N. Harakeh, Phys. Lett. B 637, 43 (2006).

[33] D. H. Youngblood, Y.-W. Lui, U. Garg and R. J. Peterson, Phys. Rev. C 45, 2172 (1992).

[34] C. Rigollet, Mod. Phys. Lett. A 25, 1955 (2010).

[35] F. Sauli, Nucl. Instr. Meth. A386, 531 (1997).

[36] Y. Giomataris, Ph. Rebourgeard, J. P. Robert, and G. Charpak, Nucl. Instr. Meth. A376, 29 (1996).

[37] Y. Shimizu, T. Kobayashi. T. Kubo, N. Chiga, T. Isobe, T. Kawabata, Y. Kondo, K. Kusaka, Y. Matsuda, T. Motobayashi, T. Murakami, T. Nakamura, J. Ohnishi, T. Ohnishi, H. Okuno, H. Otsu, H. Sakurai, H. Sato, Y. Satou, K. Sekiguchi, Y. Togano, and K. Yoneda, J. Phys.: Conf. Ser. 312, 052022 (2011).

[38] D. Suzuki, M. Ford, D. Bazin, W. Mittig, W.G. Lynch, T. Ahn, S. Aune, E. Galyaev, A. Fritsch, J. Gilbert, F. Montes, A. Shore, J. Yurkon, J.J. Kolata, J. Browne, A. Howard, A.L. Roberts, and X.D. Tang, Nucl. Instr. Meth A691, 39 (2012).

[39] C.S. Lee, S. Ota, H. Tokieda, R. Kojima, Y.N. Watanabe, and T. Uesaka, JINST 9, C05014 (2014).